

Interband spectroscopy of a quasi-three-dimensional electron gas in wide parabolic (Al,Ga)As quantum wells

M. Fritze, W. Chen, and A. V. Nurmikko

Division of Engineering and Department of Physics, Brown University, Providence, Rhode Island 02912

J. Jo, M. Santos, and M. Shayegan

Department of Electrical Engineering, Princeton University, Princeton, New Jersey 08540

(Received 29 December 1992)

The quasi-three-dimensional electron gas found in wide n -type parabolic $\text{Al}_x\text{Ga}_{1-x}\text{As}$ quantum wells has been studied through photoluminescence spectroscopy in perpendicular and in-plane magnetic fields. The conduction-band subband structure composed of several occupied closely spaced levels ($\delta E \approx 1$ meV) can be clearly identified from the spectra, aided by the sharpening of the luminescence emission into narrow peaks by Fermi-edge singularity effects (many-electron-one-hole exciton). The luminescence behavior in magnetic fields shows clearly the relative importance of the following energies in the problem: the Fermi energy, the subband spacing, the cyclotron energy, and the Coulomb perturbation by the photoholes. In the limit where the cyclotron energy dominates, an accurate measurement of the thickness of the electron slab is spectroscopically determined. A magnetic-field anomaly in the quantum limit near filling factor $\nu = \frac{2}{3}$ has been observed.

I. INTRODUCTION

The opportunity to study a quasi-three-dimensional (3D) electron gas without the limitations on its mobility imposed by bulk material has motivated most of the recent work on wide, parabolic $\text{Al}_x\text{Ga}_{1-x}\text{As}$ quantum wells (WPQW). Unusual effects have been predicted in these structures for collective excitations, such as charge and spin density waves and in the quantum Hall-Wigner solid regimes.¹⁻⁴ A number of transport studies have been conducted to yield such basic information as subband occupancy and width of the electron slab.⁵⁻¹⁰ Furthermore, the WPQW's offer the opportunity to study the breakdown of the fractional quantum Hall effect (FQHE) with increasing electron layer thickness (hence screening of the short-range Coulomb interactions),^{4,11} as well as the observation of missing plateaus in the integer quantum Hall regime due to subband degeneracies.¹² In terms of spectroscopic work, it has been shown that the inter-subband absorption probed in far-infrared (FIR) studies occurs at the bare quantum well frequency ω_0 , independent of the electron-electron interactions (in a variation of Kohn's theorem).¹³ This is due to the fact that the long-wavelength FIR probe couples only to the center-of-mass motion of the quasi-3D electron gas in these systems. Hence the FIR spectroscopy cannot directly identify the many-electron contributions in an ideal WPQW, or even the basic subband structure. A means to circumvent the problem is the introduction of spatial asymmetries by intentional introduction of impurities in order to break the translational invariance. In this way, the study of plasmons and magnetorotons has been carried out.¹⁴⁻¹⁶

Interband probes, especially by photoluminescence (PL) spectroscopy, have been used extensively in the

study of the conventional quasi-2D electron gas in square QW's and single heterojunctions.¹⁷ In contrast, very little interband spectroscopy in WPQW's has been reported to date.^{18,19} The opportunity in this case arises for a direct access to the subband structure in magnetic fields. At the same time, careful consideration must be given to the possibly complicating effects of the Coulomb perturbation by the photoholes which are a fundamental element in the recombination process. We show in this paper that such interaction effects in a WPQW give rise to a distinct, spectrally sharp structure in the PL emission which involves a many-electron-one-hole complex, in analog to the Fermi-edge singularity (FES) studied in the quasi-2D systems. While specific comparisons and a physical description of this effect is discussed in more detail below, we note that the energy scale in the binding of such a many-electron exciton is ~ 1 meV. While this is not a small perturbation, it does not hinder in the present case the identification of the subband structure on a comparable energy scale in the WPQW's.

In the presence of magnetic fields, the PL spectra show behavior which can be divided roughly into three regimes: (i) the low-field regime where the FES many-body exciton dominates, (ii) an intermediate field where complex Landau-level-subband intersection effects are observed, and (iii) a high-field regime where the cyclotron energy is the dominant energy in the problem. In regimes (ii) and (iii), we find a good phenomenological and quantitative connection to recent theoretical work by Hembree *et al.*,²⁰ who studied the WPQW problem in magnetic fields for the conduction-electron system alone.

II. EXPERIMENTAL ARRANGEMENT

The samples were grown by molecular-beam epitaxy so that a parabolic section of about 2000 Å in thickness was

formed by grading an $\text{Al}_x\text{Ga}_{1-x}\text{As}$ layer quadratically across the well.^{5,6,21} The electrons were introduced from two remote doping regions outside the well. As has been well documented, the Hartree contribution to the total potential by a uniform slab distribution of electrons in the well ($\phi = -e^2nz^2/2\epsilon$) can cancel the compositional potential so that the net potential is flat (square-well-like) over the well.^{5,6,8,9} The typical uniform electron thickness in such a quasi-3D slab is 1000 Å. In one of our samples (denoted by M_2), for example, the Al concentration x varied quadratically across the 2000-Å layer in the growth direction (z) from $x=0$ at $z=0$ in the middle of the well, to $x=0.19$ at the edges of the well ($z=\pm 1000$ Å). Modulation doping was implemented by δ doping with Si outside the parabolic section with a spacer layer of 165 Å.^{5,6} The subband structure in the conduction band is calculated by taking into account the three potential terms: the compositional parabolic potential, the Hartree potential due to the electron gas, and the exchange-correlation potential:

$$V^{\text{tot}} = V_{\text{comp}} + V_{\text{Hartree}} + V_{\text{xc}}.$$

We have solved the Schrödinger and Poisson equations self-consistently for our structures and found typical subband separations of $\delta E \sim 1-2$ meV with multiple (four or five) subbands occupied.^{17,18} An example of such calculations is shown schematically in Fig. 1, including the simple envelope wave functions which show the conservation of parity by symmetry in an idealized WPQW. Some of the interband optical transitions discussed below are also indicated ($A-D$). As is well known, the addition of the electron gas has the effect of flattening the compositional

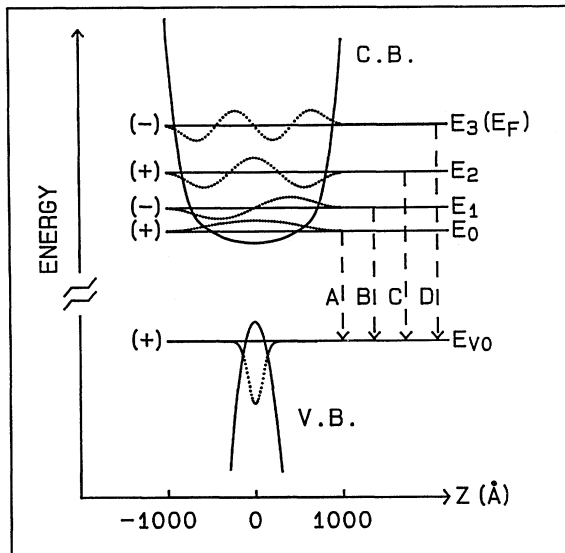


FIG. 1. Calculated band-structure diagram with wave functions for a typical WPQW (M_2). Note the symmetry of the structure, making parity a good quantum number. Also note the nearly square well shape of the conduction band due to the self-consistent solution, including Hartree and exchange terms. The optical transitions observed are indicated by dashed lines.

potential to approximate that of a wide square well. We note that the subband structure of wide WPQW's in perpendicular and parallel magnetic fields has also been calculated, predicting a wealth of subband depopulation and level crossing effects.^{20,22,23} In general the WPQW's contrast with the typical quasi-2D systems in that the bare well, Hartree, the exchange-correlation potentials are all of comparable magnitude.²⁰ In addition, the cyclotron energy (approximately 1.7 meV per tesla) can be easily comparable to the subband spacing in moderate magnetic fields, leading to novel behavior.

The photoluminescence spectroscopy was performed mostly at $T=0.5$ K, with magnetic fields applied both in perpendicular (z) and parallel (x - y) configurations with respect to the QW layer plane. The experiments were carried out in a He^3 refrigerator in a 13-T superconducting magnet, equipped with fiber optic access, and followed by a spectrometer with multichannel CCD optical detection. Both He-Ne lasers and infrared semiconductor laser diodes were used as excitation sources. The PL measurements were accompanied by simultaneous transport measurements in order to test for the light sensitivity of various samples. We have found that many samples, in which persistent photoconductivity effects are useful in tuning the electron density for transport measurements, were simply too light sensitive for PL experiments at low temperatures. Small incident powers ($< 10^{-6}$ W focused to a 200- μm spot) of He-Ne laser irradiation caused large depletions of the carrier density. This behavior may be related to displacement of the Fermi level by impurities in the superlattice buffer layer found generically in such samples. Consequently, samples without a superlattice buffer were found most useful in this work.

III. EXPERIMENTAL RESULTS

Table I summarizes the salient parameters of the three (light insensitive) samples M_1 , M_2 , and M_3 used in our studies. In their electronic character they span a range of occupancy and electron slab thickness from a thick quantum well ($t=600$ Å) to a quasi-3D electron gas ($t > 1000$ Å). The specific curvatures of the parabolic profiles in terms of the Al concentration at the well edges were as follows: for sample M_1 , $x=0.20$ for a well width of $W=1500$ Å; for samples M_2 and M_3 , $x=0.19$ for $W=2000$ Å. Figure 2 shows the calculated subband energies for a typical sample (M_2 , with an Al concentration reaching 0.19 at the edges of the 2000-Å-thick well) as a function of the carrier density, obtained from the self-consistent calculations. Note how the subband energy

TABLE I. Physical parameters of the three (Al,Ga)As WPQW samples used in this study.

Sample	n_s (cm^{-2})	Subbands	Slab thickness	Mobility ($\text{cm}^2/\text{V sec}$)
M_1	1.7×10^{11}	1	600 Å	1.6×10^5
M_2	2.5×10^{11}	4	1000 Å	1.2×10^5
M_3	2.9×10^{11}	5	1200 Å	5×10^4

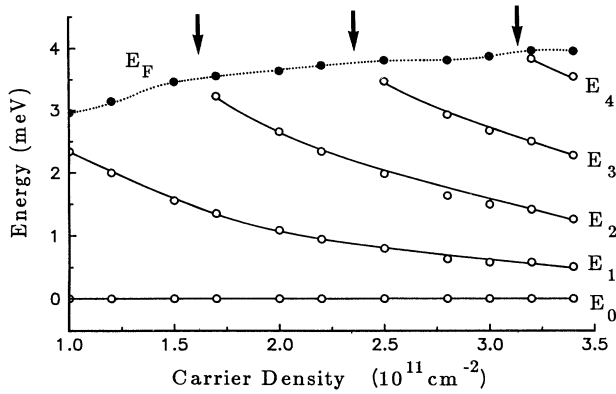


FIG. 2. Calculated conduction-band energies vs carrier density for a WPQW with a typical curvature ($M2$ and $M3$). Note the decreasing subband energy spacings with increasing carrier density (corresponding to wider electron slabs). Also note the constant Fermi level once the well has reached its design density. The arrows indicate the onset of an additional occupied subband with increasing carrier density.

separation decreases with increasing sheet carrier density. This characteristic feature is due to the fact that in a WPQW the thickness of the electron slab increases with sheet carrier density. Also note how the Fermi level remains constant with increasing areal electron density once the well has reached its design density: another basic property of the WPQW's.

A. Zero magnetic-field photoluminescence spectra

Figure 3 shows schematically various possibilities for radiative recombination paths by which electrons in the

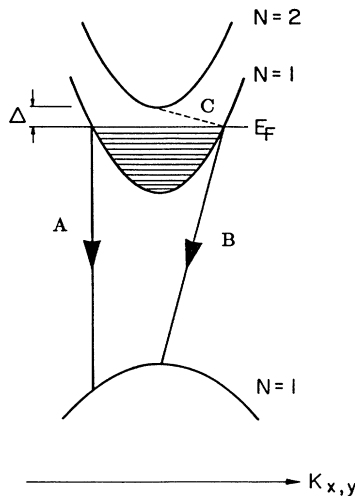


FIG. 3. k -space diagram of the optical transitions involved at the Fermi level (only two subbands have been included for simplicity). Process A corresponds to direct electron-hole transitions. Process B corresponds to indirect transitions involving recoil of the Fermi sea or impurities. Process $B+C$ represents virtual scattering from E_F to a nearby empty subband, thus allowing electrons at E_F to couple to holes at $k=0$. This process is responsible for the observation of the FES in WPQW's.

WPQW participate with injected photoholes at the lowest valence subband (under low-level illumination conditions, the excess electron density is many orders of magnitude below the equilibrium density). For simplicity this schematic highlights the proximity of a single electric subband ($n=2$) to the Fermi level. In terms of the possible radiative recombination processes in such a case, one must generally consider three different transitions. The first involves the direct transitions of electrons and holes at the same k vector (process A in Fig. 3). The second accounts for the impurity-assisted indirect transitions or those which require a recoil for the Fermi sea (process B). The third corresponds to the $N=2$ exciton-assisted FES induced by the resonant coupling of the two states (processes $B+C$). It is this last key process that endows the PL spectra with a many-body exciton character as discussed below. Apart from enhancing the recombination process, this circumstance enables us also to study the excitonic enhancement of the FES involving the electrons at $k \approx 0$ at low temperature and a low excitation level.

Figure 4 shows a series of PL spectra at $T=0.5$ K for the three samples $M1$, $M2$, and $M3$ both at zero magnetic field (top traces) and in a small perpendicular field (bottom traces). The zero-field spectrum of $M1$ looks very similar to those observed in typical square (quasi-2D) QW's, with a peak at the $n=1$ subband edge and a high-energy fall-off due to k conservation and decreasing hole population at larger k values. The spectra for samples $M2$ and $M3$, in contrast, look quite different. Several distinct features which indicate the number of occupied conduction subbands are seen, superposed on an envelope that reaches its maximum at high energy. It is highly unlikely that shallow defects are present in these spectra, based on our extensive studies of these samples. (For example, the number of peaks observed for samples $M2$ and $M3$, four and five, respectively, fully agree with the num-

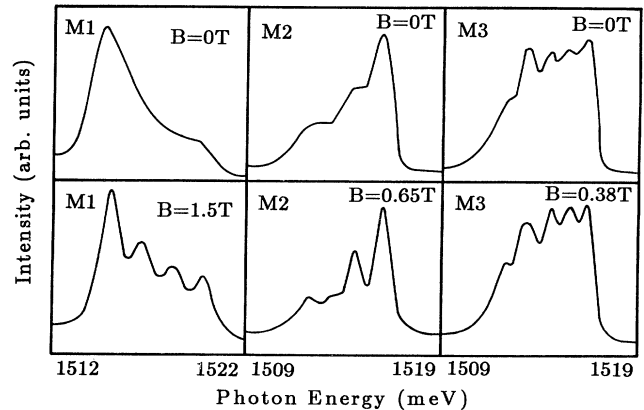


FIG. 4. PL spectra at $T=0.5$ K of samples of the three WPQW's: $M1$, with only one occupied subband, shows a conventional PL line shape; $M2$ and $M3$, with multiple closely spaced subbands occupied, both have their spectral weight centered near E_F . The bottom panels show Landau-level (LL) structure for $M1$, and subband structure for $M2$ and $M3$ in small applied B fields.

ber of occupied conduction band levels for these samples as confirmed by transport experiments. They also completely agree with our self-consistent calculations for the number of occupied subbands expected for $M2$ and $M3$. Note that E_F is approximately the same for all three samples, despite their increasing sheet carrier density (from $M1$ – $M3$). The only effect of increasing areal carrier density is to reduce the subband energy spacing and the population of more subbands. This behavior, where the electron slab thickness increases with sheet carrier density while leaving E_F nearly constant, is expected from the self-consistent calculations referred to above. This is, of course, in contrast to the dependence of E_F on carrier density in the conventional (nonparabolic) quasi-2D case. The energy separation of the peaks and features in Fig. 4 of about $\delta E \approx 1$ meV is also in good agreement with the calculations as well as transport measurements for the subband structure. Thus, in spite of the complication of the Coulomb perturbation by the photoholes, the separation of the PL peak energy positions yields useful information about the single-particle band structure of the WPQW's.

We now consider the further implications of the spectra in Fig. 4 from the standpoint of the FES phenomena. As observed, the envelope of the PL amplitude rises steadily for samples $M2$ and $M3$, reaching a peak value for the conduction electrons at $E = E_F$. Such an overall spectral tendency is difficult to explain using the single-particle wave functions highlighted in Fig. 1. For example, in the case of sample $M2$ the fourth subband contains few electrons and is parity forbidden (vs recombination with the lowest hole subband), yet the overall PL emission reaches maximum at this energy.¹⁸ Such a high-energy enhancement is observed only for samples where closely separated ($\delta E \approx 1$ meV) multiple subbands are occupied by electrons. In addition, the high-energy enhancement is also a very temperature sensitive effect, as seen for sample $M2$ in Fig. 5. Note how the overall

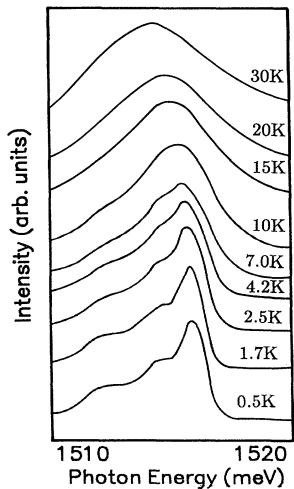


FIG. 5. PL spectra of sample $M2$ as a function of temperature. Note the disappearance of the high-energy enhancement by $T = 10$ K.

envelope shape reverts back to conventional appearance by about $T \approx 10$ K, while the distinct spectral features, indicative of the subbands, also disappear.

We ascribe the prominent high-energy enhancement and the distinct spectral features for samples $M2$ and $M3$ to the formation of a Fermi-edge singularity, i.e., many-electron–one-hole complex in these structures. In a recent paper we have presented initial data while suggesting such an interpretation.¹⁸ This is supported by the strong temperature dependence of the PL spectra as well as their behavior in magnetic fields (see below). The temperature dependence of the FES is consistent with a binding energy of about 1 meV for this many-body exciton complex. On the one hand, this gives rise to distinct spectra in analog to excitons in undoped quantum wells; on the other hand, the Coulomb perturbation is small enough that useful information on the conduction-electron subband structure can be obtained. Furthermore, already in moderate magnetic fields (~ 1 T) the electron-hole Coulomb interaction is suppressed in favor of free-particle magnetic quantization effects.

The mechanism of the formation of the FES in the WPQW's, as viewed through radiative recombination, is similar to effects studied recently in asymmetric square quantum wells (SQW's) with dominant contributions by near-resonant higher conduction subbands.^{24–26} In the SQW case, the proximity of the Fermi level to a higher unoccupied ($n = 2$) conduction subband (within a few meV) permits intersubband scattering to intermediate the electron-hole Coulomb interaction, allowing thermalized photoholes at $k = 0$ to couple electrons of larger wave vector.^{27–29} For purposes of comparison, in Fig. 6 we show PL spectra from a GaAs SQW in the energy range corresponding to the vicinity of the $n = 2$ conduction subband, with a FES peak clearly distinct (long arrow) due to the proximity of the second conduction subband (short

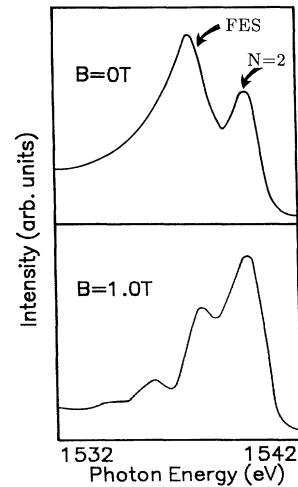


FIG. 6. PL spectra at $T = 0.5$ K for an asymmetric SQW sample in the vicinity of E_F . Note the clear FES peak made possible by virtual scattering from E_F to the nearly empty $N = 2$ subband level. The bottom panel shows the enhancement of the LL amplitudes in the vicinity of E_F due to the FES effect.

arrow). The binding energy of the FES in this case has been determined to be approximately 0.7 meV.²⁶ In the case of initially free holes, the FES can only be observed due to the higher subband proximity effect. However, the FES aspect can also be observed in systems with very large effective hole masses (such as in $\text{In}_x\text{Ga}_{1-x}\text{As}$ SQW's where the holes are localized due to alloy potential fluctuations).³⁰ In the case of WPQW's, the conditions can naturally occur where conduction-subband energy separation occurs on a scale of 1 meV, with E_F typically also only a few meV. This permits the intersubband scattering to occur among all the occupied conduction subbands and nearby higher unoccupied levels so that the FES effect can penetrate across the entire Fermi sea. As a consequence, excitonlike sharp spectral structure can be seen at energies which mirror the occupied conduction-subband structure, superposed on an envelope which reaches a maximum at the high-energy edge, at E_F (zero-field spectrum in Fig. 4).

As already mentioned, the PL spectra of Fig. 4 are also puzzling due to the apparent violation of parity selection rules (as both the even and odd conduction-subband edges are discernable). We are unsure of the specific reason for the breakdown of parity, but conjecture that weak structural asymmetries (inhomogeneities) and the very small hole subband separation is responsible, aided perhaps by the electron-hole Coulomb interaction. In a given sample, the spectral features are highly reproducible, for instance the anomalously large $n=2$ subband transition in sample *M2*. Other indications suggest that sample *M2* is of excellent structural quality so that the parity violations observed here should not be viewed as influencing our results detrimentally.

B. Perpendicular magnetic fields

The bottom trace of Fig. 4 already showed the PL spectral for samples *M1*, *M2*, and *M3* in small perpendicular magnetic fields. For the conduction electrons, this field range corresponds to the case $h\omega_c < \Delta E_i$, E_F , where ΔE_i is the subband separation energy. For sample *M1* where only one conduction subband is occupied, the spectra show incipient Landau quantization with no anomalies. On the other hand, for samples *M2* and *M3* the Landau quantization is not observable; rather the spectral structure is entirely due to the conduction subbands and shows four occupied levels for *M2* and five levels for *M3*. When compared with the zero-field case, the spectra for samples *M2* and *M3* show the subband structure with further clarity. Note that in the low-field range the cyclotron energy does not yet exceed the binding energy of the FES. Hence the many-body exciton character in the recombination process is still present so that any incipient Landau quantization simply adds to the spectral sharpness of the individual subband transitions. Here we note an analog in the case of a quasi-2D SQW, with an $n=2$ conduction subband proximity enhancement, to the problem of a FES in a weak magnetic field. The bottom trace of Fig. 6 shows spectra in a GaAs SQW where Landau levels are only visible in the spectral region near the resonantly enhanced FES emission.^{25,26} In this case,

similar to the WPQW spectra, the single-particle aspect of the band structure chiefly determines the position of the spectral peak energies, while the many-body effect intrinsic to the FES determines the (enhanced) amplitude and spectral shape of the luminescence.

Figure 7 displays a series of PL spectra for sample *M3* for various perpendicular magnetic fields, well beyond the low-field regime. Note again the distinct five subband contributions in the zero- and low-field cases. With increasing magnetic field, the number of peaks, as well as their energy of emission and linewidth, all change so that the spectrum at $B=3.6$ T bears little resemblance to the zero-field emission. Two aspects can be immediately recognized from this spectral evolution in the B field, namely that Fermi level-subband crossings with commensurate depopulation are taking place, and that the PL enhancement at the high-energy edge occurs periodically with increasing field. The periodic high-energy enhancements are due to the FES effect being especially favored when higher subband levels come into (Coulomb) scattering resonance with the highest occupied level. This aspect in WPQW's is discussed in further detail in a recent publication.¹⁸ Figure 8 summarizes the spectral shifts of the transition energies in perpendicular fields for the sample *M3*. In this fanplot, lines have been added to guide the eye. The figure is very useful in appreciating the apparently complex behavior of the spectra in Fig. 7. At low magnetic fields ($B < 0.5$ T) the emission energies shift very little, indicative of the dominance of the (FES) excitonic component in the recombination process. The small shifts are thus analogous to the diamagnetic shifts of a conventional exciton. As the cyclotron energy begins to dominate the electron-hole Coulomb energy, however, the shifts indicate clearly that the spectral structure of Landau-level-like in origin ($B > 0.5$ T). The level crossings displayed in the figure reflect the complexity of the circumstance which ensues here from the crossing of the various Landau levels from different conduction subbands. Note that both the subbands and the Landau levels are involved in the B -field-induced level depopulation

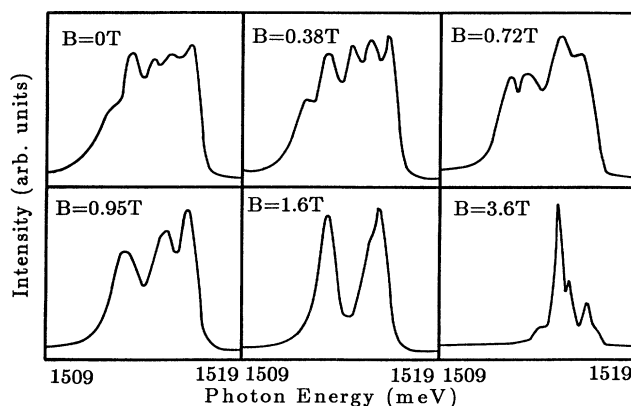


FIG. 7. PL spectra for sample *M3* at $T=0.5$ K in a perpendicular magnetic field. The subband structure is clearly evident in these spectra (five levels occupied at low fields). Spectral changes originate from subband crossings and level depopulations.

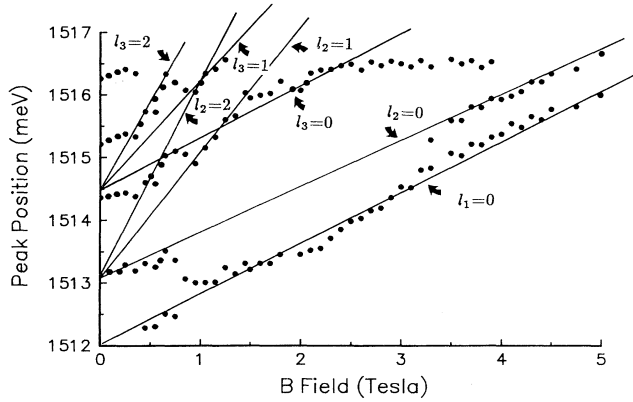


FIG. 8. Plot of the PL transition energies in perpendicular fields (dots) for sample *M3*. The Landau fans (solid lines drawn to guide the eye) extrapolate well to the zero-field subband energies.

due to the small subband energy separations. This aspect, which is a specific property of the WPQ's, leads to a highly "nonlinear" fan diagram. The Landau "fans" drawn through the data points all extrapolate to the five subband edges in zero field, in good agreement with the five subbands being occupied as verified in transport measurements. As one finite deviation from expected (one electron) Landau fans, we note that the lines indicative of the $l_1=0$ and $l_2=0$ are not entirely parallel. Both the optical and the transport data also support each other in assigning a value of about $\delta E \approx 1$ meV to the conduction-subband separation. Beyond approximately $B > 5$ T, the PL emission is composed of one dominant feature only, as the quantum limit ($n=1$; $l=0$) is being approached.

As noted in Sec. I, the subband structure of a WPQ in a perpendicular magnetic field has been calculated.²⁰ The behavior was described in terms of three field regimes, depending on the relative magnitude of δE , $\hbar\omega_c$, and E_F . The calculations predict a nearly constant E_F in low fields, complex Landau-level-subband depopulation effects in intermediate fields, and simple subband level depopulation effects (between the lowest Landau levels) in the high-field regime. Notwithstanding the complication of the electron-hole Coulomb interaction, these theoretical predictions are well verified in our PL experiments. Finally, it should be remarked that the underlying physics for an electron gas in a WPQ makes the perpendicular magnetic-field case a highly self-consistent problem. Since the odd and even conduction subbands are depopulated sequentially, the total thickness of the electron slab is expected to oscillate in the B field.²⁰ Furthermore, in the very high-field case (quantum limit), the wave functions are strongly distorted from their lower field orbitals due to the requirement that the electron slab screens the parabolic potential.³¹ This field regime is discussed further in Sec. IV.

We also need to make additional remarks about the interband nature of our PL probe in the context of the participating hole states and the applicable selection rules. If we assume that at the measurement temperatures

($T=0.5$ K) only the lowest hole subband is occupied, we find the puzzle that the Landau-level selection rule appears to be violated as several conduction subbands are clearly making up the Landau fans. The apparent violation can be understood as follows. For a conduction-subband separation of ≈ 1 meV, the hole subband spacing is only a fraction of a meV in our WPQ's, taking into account the hole effective mass in $\text{Al}_x\text{Ga}_{1-x}\text{As}$. (The ratio of electron and hole Landau-level spacings goes as the ratio of their effective masses). We can well envision a finite coupling of the hole subbands which are due to symmetry-breaking inhomogeneities and/or impurities in the samples.

C. In-plane magnetic fields

The application of in-plane magnetic fields (B_{\parallel}) provides a useful geometry for the determination of the thickness of the electron slab in the WPQ's by luminescence spectroscopy. In the conventional quasi-2D SQW case, a low or moderate in-plane field has little effect on the optical spectra due to the small perpendicular envelope function spatial extent (typically < 100 Å). With increasing B_{\parallel} , hybrid electric-magnetic levels are eventually formed which merge smoothly into Landau levels at high fields. The wide parabolic wells show strong contrasts in their in-plane response. The closeness in the energy spacing of the conduction subbands implies that both the subbands and Landau levels are involved in magnetic depopulation, and that the transition to Landau-level-dominated behavior can be observed at relatively low fields.²² Figure 9 shows a series of spectra for the sample *M2* for a range of in-plane fields. Note how subband depopulation and level crossings are clearly evident (e.g., in analogy to Fig. 7) and that these processes take place at modest values of B_{\parallel} . As in the case of perpendicular fields, the exciton aspect complicates the spectral line shapes only at the very lowest fields. Considerable information can again be readily obtained by graph-

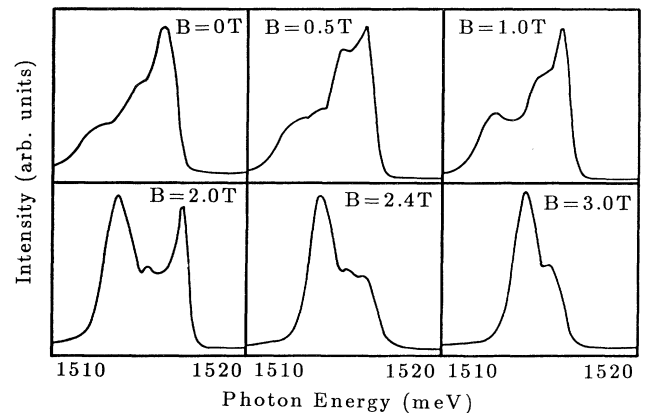


FIG. 9. PL spectra at $T=1.2$ K for sample *M2* as a function of the in-plane magnetic field. Note the large changes in the spectra already evident at low- B fields ($B=1.0$ T). The level crossing and depopulation effects observed in low and moderate magnetic fields can be used to measure the thickness of the electron slab.

ing the spectral shifts for the range of measured B_{\parallel} values. Figure 10 is a fanplot of the transition energies as a function of B_{\parallel} (the energies were obtained from the spectral positions of the PL peaks). There are clearly two regimes corresponding to $h\omega_c < \delta E_{\text{subband}}$ and $h\omega_c > \delta E_{\text{subband}}$. We note that $h\omega_c = 0.85$ meV for $B = 0.5$ T. This is comparable to the subband energies in our WPQW systems on the order of 1 meV. Thus our data show little shift for fields $B < 0.5$ T. A shift toward Landau behavior occurs for $B > 0.5$ T. The transition region is clearly visible for the third subband transition, which changes smoothly to the l_0 level by the field $B = 4.0$ T. We note explicitly here that for the field range displayed ($B \leq 5$ T) we are still in the transitional regime of electric to Landau-level behavior. Nonetheless, the plot shows clearly how the transition to Landau-type behavior with increasing field takes place already at $B_{\parallel} = 0.47$ T, this field value obtained from the rather abrupt change of slope for the third conduction subband where the data points fall on the $l_2 = 2$ Landau level (indicated by the arrow in the figure). For $B_{\parallel} = 0.47$ T, we obtain a cyclotron diameter of 1024 \AA which hence gives us a direct optical method to measure the electron slab's thickness. The value of 1024 \AA agrees well with those obtained previously from transport measurements on this sample.^{6,7} The electron slab thicknesses obtained by the in-plane luminescence measurements for the samples $M1$ and $M3$ were 630 and 1148 \AA , respectively, as summarized in Table I. Note that with increasing sample thickness, more subbands are occupied as expected as a general feature of our WPQW's. Again, the Fermi level remains fairly constant with increasing sheet carrier density, due to the compensating effect of increase in the thickness of the electron slab. Above $B_{\parallel} > 0.5$ T, the transitions approach a dominant Landau-type character, with level crossings and subband populations occurring similarly to the perpendicular field case. We are here in the hybrid electric-magnetic regime, where the levels approximately extrapolate to the z-subband levels.²² For the higher-field regime ($B > 5$ T), the levels approach true

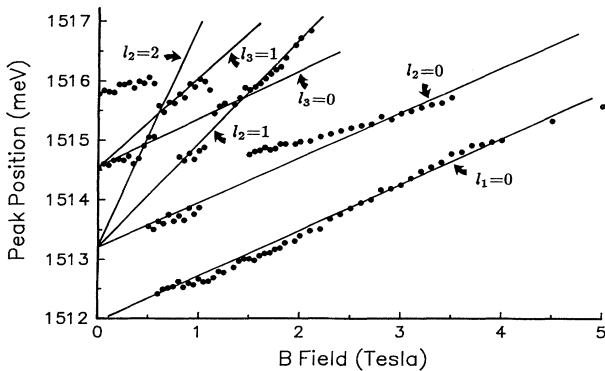


FIG. 10. Plot of the PL transition energies in parallel fields for sample $M2$ (dots) with solid lines guiding the eye for Landau-level transitions. Note that the transition to Landau behavior occurs at low- B fields ($B = 0.4$ T). This change was used to measure the thickness of all the WPQW samples.

Landau-level character, and extrapolate to a single bulk level as expected for a quasi-3D system.

D. High magnetic-field regime (quantum limit $\nu = \frac{2}{3}$)

The WPQW's offer an interesting case in the study of the quantum Hall effect both in the integer and fractional (FQHE) regimes. The observed breakdown of the FQHE in transport studies^{4,11} has been attributed to the effect of dimensionality in the sense of increased screening of the short-range many-electron Coulomb interactions in the WPQW's. At the same time, PL spectroscopy of a quasi-2D electron gas in the FQHE regime has yielded a range of phenomena where either anomalous amplitude³² or spectral shifts³³ has been observed near particular fractional filling factors ν . A major contemporary question in the applicability of a PL measurement to augment transport experiments is the question of the impact of the electron-hole Coulomb interaction on the 2D electron gas. Here we wish to briefly introduce initial results of PL spectroscopy from the WPQW samples discussed above to show observations which are similar to those seen recently in quasi-2D SQW's. A fuller accounting of these results will be given elsewhere.

We focus on PL spectra obtained on the sample $M2$ in a perpendicular field in the range of $12 < B < 23$ T. For the well-established subband parameters and the electron density, the electron gas should readily reach the quantum limit in this field range, with only one Landau level of the lowest subband occupied ($n = 1, l = 0$). The PL spectra at $T = 0.5$ K show the emergence and appearance of a distinct high energy satellite feature whose amplitude variations are correlated with the amplitude variations of the main peak. Examples of the field-dependent spectral variations for this doublet are shown in Fig. 11 for $B = 10, 15,$ and 20 Tesla at $T = 0.5$ and 1.2 K. Note that the individual peak widths are on the order of 0.5 meV, and that while the relative doublet amplitude varies strongly with field at $T = 0.5$ K, the higher-energy peak is considerably attenuated at $T = 1.2$ K and shows much

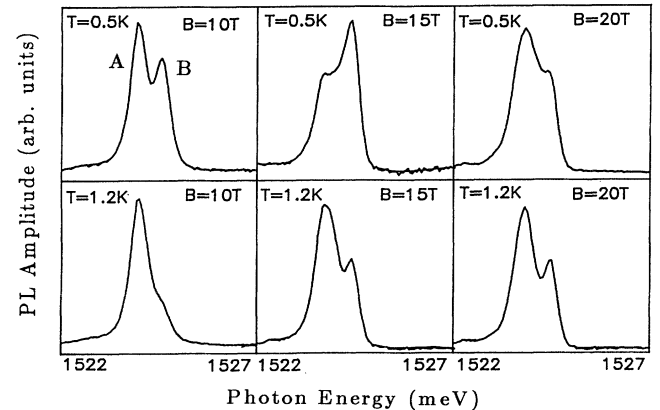


FIG. 11. PL spectra for sample $M2$ in the high magnetic-field regime. Note the emergence of a spectral doublet with the high-energy peak reaching a maximum near $\nu = \frac{2}{3}$ (at 15.5 T). The high-energy peak disappears by $T \sim 1.2$ K.

less field dependence than at $T=0.5$ K. At even higher temperatures, the high-energy feature is obliterated altogether. Figure 12 shows the amplitude variation of the two components of the doublet as a function of the field. Note how the maximum in the high-energy component (and minimum of the main component) is reached at $B = 15.5$ T, a value which also corresponds to the filling factor $\nu = \frac{2}{3}$.

We conjecture (and will present further results elsewhere) that the doublet structure shown in Fig. 11 is associated with a FQHE state with $\nu = \frac{2}{3}$. Similar doublet structure and behavior was also verified for the sample *M1* but not for *M3*. However, sample *M3* has a substantially lower mobility. It is interesting to note that such doublet structures associated with the $\nu = \frac{2}{3}$ and $\frac{1}{3}$ filling factors have been reported in the PL spectra obtained both from SQW's and single heterojunction structures in recent literature.^{34–37} In these reports, anomalous amplitude variations similar to and occurring over a field range comparable to that in Fig. 6 have been argued to make the PL observations indicative of the FQHE state. The real physical situation is, of course, complicated by the poorly understood role of the photoholes in the quantum limit in terms of the perturbation of the FQHE state on the one hand, and on the other by the structure of the hole state which participates in the recombination event. We are presently exploring these questions in the WPQW's.

Finally, we wish to point out the similarity with the PL spectroscopy in our WPQW's and the recent work attempting to identify FQHE states in either single quantum wells or heterojunctions.^{32,33} The experimental conditions in all cases are such that a couple of closely spaced conduction subbands are at issue for a Fermi energy of a few meV. The Fermi-edge singularity effects, resonantly enhanced by the subband structure, are likely to be present in these other experiments as well.³⁸ One important difference, however, is the spatial location of the photohole (wave-function overlap): in the WPQW's the hole attains maximum probability amplitude in the middle of the well.

IV. SUMMARY

Wide parabolic quantum wells have been studied by interband magnetoluminescence spectroscopy. The subband structure of the wide (quasi-3D) electron slabs has been directly observed in the low-temperature ($T=0.5$ K)

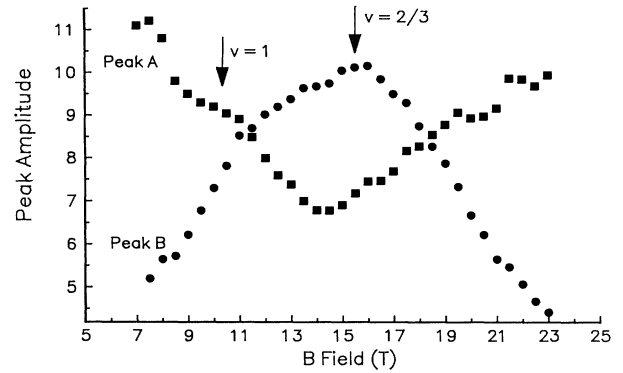


FIG. 12. Amplitude of peaks *A* and *B* in magnetic field, indicating a maximum in the high-energy doublet component near $\nu = \frac{2}{3}$. The maximum of peak *B* corresponds to a minimum of peak *A*.

PL spectra. Subband separations of $\delta \approx 1$ meV were observed, in agreement with self-consistent calculations for these structures. We also verified the fact that the electron slab thickness increases with increasing carrier density at constant E_F . Many-body exciton effects were witnessed in the overall spectral envelope structure and the presence of sharp subband recombination features. The temperature dependence of such a Fermi-edge singularity behavior was shown to be consistent with many-electron–one-hole binding energies of about 1 meV. This relatively small Coulomb energy made it possible to obtain direct insight into the conduction-electron subband behavior in quantizing magnetic fields, and use in-plane fields to measure the electron slab thickness. The high-field anomaly near filling factor $\nu = \frac{2}{3}$ is subject to ongoing study.

ACKNOWLEDGMENTS

This work was supported by the National Science Foundation Grants Nos. DMR-9112329 and DMR-9121747. The authors wish to thank Pawel Hawrylak for very useful discussions. Part of this work was performed at the Francis Bitter National Magnet Laboratory at MIT, supported by the National Science Foundation. We are especially grateful to Don Heiman for his exper-

¹L. Brey, Phys. Rev. B **40**, 11 634 (1989).

²A. H. MacDonald and G. W. Bryant, Phys. Rev. Lett. **58**, 515 (1987).

³B. Halperin, Jpn. J. Appl. Phys. **26**, Suppl. 26-3, **1913** (1987).

⁴S. He, F. C. Zhang, X. C. Xie, and S. Das Sarma, Phys. Rev. B **42**, 11 376 (1990).

⁵M. Shayegan, T. Sajoto, M. Santos, and C. Silvestre, Appl. Phys. Lett. **53**, 791 (1988).

⁶T. Sajoto, J. Jo, M. Santos, and M. Shayegan, Appl. Phys. Lett.

55, 1430 (1989).

⁷T. Sajoto, J. Jo, L. Engel, M. Santos, and M. Shayegan, Phys. Rev. B **39**, 10 464 (1989).

⁸A. J. Rimberg and R. M. Westervelt, Phys. Rev. B **40**, 3970 (1989).

⁹E. G. Gwinn, P. F. Hopkins, A. J. Rimberg, and R. M. Westervelt, Phys. Rev. B **41**, 10 700 (1990).

¹⁰P. F. Hopkins, A. J. Rimberg, E. G. Gwinn, R. Westervelt, M. Sundaram, and A. C. Gossard, Appl. Phys. Lett. **57**, 2823

- (1990).
- ¹¹M. Shayegan, J. Jo, W. Suen, M. Santos, and V. J. Goldman, *Phys. Rev. Lett.* **65**, 2916 (1990).
- ¹²K. Ensslin, M. Sundarum, A. Wixforth, J. H. English, and A. C. Gossard, *Phys. Rev. B* **43**, 9988 (1991).
- ¹³L. Brey, N. F. Johnson, and B. I. Halperin, *Phys. Rev. B* **40**, 10 647 (1989).
- ¹⁴K. Karrai, H. D. Drew, M. W. Lee, and M. Shayegan, *Phys. Rev. B* **39**, 1426 (1989); K. Karrai, M. Stopa, X. Ying, H. D. Drew, S. Das Sarma, and M. Shayegan, *ibid.* **42**, 9732 (1990).
- ¹⁵K. Karrai, X. Ying, H. D. Drew, M. Santos, M. Shayegan, S. R. E. Yang, and A. H. MacDonald, *Phys. Rev. Lett.* **67**, 3428 (1991).
- ¹⁶X. Ying, K. Karrai, H. D. Drew, M. Santos, and M. Shayegan, *Phys. Rev. B* **46**, 1823 (1992).
- ¹⁷A. Wixforth, M. Sundarum, K. Ensslin, J. H. English, and A. C. Gossard, *Phys. Rev. B* **43**, 10 000 (1991).
- ¹⁸M. Fritze, W. Chen, A. V. Nurmikko, J. Jo, M. Santos, and M. Shayegan, *Phys. Rev. B* **45**, 8408 (1992).
- ¹⁹J. H. Burnett, H. M. Cheong, W. Paul, P. F. Hopkins, E. G. Gwinn, A. J. Rimberg, R. M. Westervelt, M. Sundarum, and A. C. Gossard, *Phys. Rev. B* **43**, 12 033 (1991).
- ²⁰C. E. Hembree, B. A. Mason, A. Zhang, and J. A. Slinkman, *Phys. Rev. B* **46**, 7588 (1992).
- ²¹M. Sundarum, A. C. Gossard, J. H. English, and R. M. Westervelt, *Superlatt. Microstruct.* **4**, 683 (1988).
- ²²M. P. Stopa and S. Das Sarma, *Phys. Rev. B* **40**, 10 048 (1989).
- ²³M. P. Stopa and S. Das Sarma, *Phys. Rev. B* **47**, 2122 (1992).
- ²⁴W. Chen, M. Fritze, A. V. Nurmikko, C. Colvard, D. Ackley, and H. Lee, *Phys. Rev. Lett.* **64**, 2434 (1990).
- ²⁵W. Chen, M. Fritze, A. V. Nurmikko, M. Hong, and L. L. Chang, *Phys. Rev. B* **43**, 14 738 (1991).
- ²⁶W. Chen, M. Fritze, W. Walecki, A. V. Nurmikko, D. Ackley, M. Hong, and L. L. Chang, *Phys. Rev. B* **45**, 8464 (1992).
- ²⁷J. F. Mueller, *Phys. Rev. B* **42**, 11 189 (1990); J. F. Mueller, A. Ruckenstein, and S. Schmitt-Rink, *Mod. Phys. Lett.* **5**, 135 (1991).
- ²⁸P. Hawrylak, *Phys. Rev. B* **42**, 8986 (1990).
- ²⁹P. Hawrylak, *Phys. Rev. B* **44**, 6262 (1991).
- ³⁰M. S. Skolnick, J. M. Rorison, K. J. Nash, D. J. Mowbray, P. R. Tapster, S. J. Bass, and A. D. Pitt, *Phys. Rev. Lett.* **58**, 2130 (1987).
- ³¹L. Brey, *Phys. Rev. B* **44**, 3772 (1991).
- ³²B. B. Goldberg, D. Heiman, A. Pinczuk, L. Pfeiffer, and K. West, *Phys. Rev. Lett.* **65**, 641 (1990); A. J. Turberfield, S. R. Haynes, P. A. Wright, R. A. Ford, R. G. Clark, J. F. Ryan, J. J. Harris, and C. T. Foxon, *ibid.* **65**, 637 (1990).
- ³³H. Buhmann, W. Joss, K. Von Klitzing, I. V. Kukushkin, G. Martinez, A. S. Plaut, K. Ploog, and V. B. Timofeev, *Phys. Rev. B* **65**, 641 (1990).
- ³⁴E. M. Goldys, S. A. Brown, R. B. Dunford, A. G. Davies, R. Newbury, R. G. Clark, P. E. Simmons, J. J. Harris, and C. T. Foxon, *Phys. Rev. B* **46**, 7957 (1992).
- ³⁵R. G. Clark, R. A. Ford, S. R. Haynes, J. F. Ryan, A. J. Turberfield, P. A. Wright, C. T. Foxon, and J. J. Harris, in *High Magnetic Fields in Semiconductor Physics III*, edited by G. Landwehr, Springer Series in Solid State Sciences Vol. 101 (Springer-Verlag, Berlin, 1992), p. 231.
- ³⁶B. B. Goldberg, D. Heiman, A. Pinczuk, L. Pfeiffer, and K. West, in *High Magnetic Fields in Semiconductor Physics III* (Ref. 35), p. 243.
- ³⁷B. B. Goldberg, D. Heiman, A. Pinczuk, L. Pfeiffer, and K. West, *Surf. Sci.* **263**, 9 (1992).
- ³⁸J. M. Calleja, A. R. Goni, B. S. Dennis, J. S. Weiner, A. Pinczuk, S. Schmitt-Rink, L. Pfeiffer, K. W. West, J. F. Muller, and A. E. Ruckenstein, *Solid State Commun.* **79**, 911 (1991); in *Optics in Nanostructures*, edited by F. Henneberger, S. Schmitt-Rink, and E. O. Göbel (Akademie Verlag, Berlin, 1993), p. 335.